Wave simulation in partially frozen porous media with fractal freezing conditions

José M. Carcione[a)]
Istituto Nazionale di Oceanografia e di Geofisica Sperimentale (OGS), Borgo Grotta Gigante 42c, 34010 Sgonico, Trieste, Italy

Juan E. Santos
Facultad de Ciencias Astronómicas y Geofísicas, Universidad Nacional de La Plata, Paseo del Bosque, s/n, 1900 La Plata, Argentina and Department of Mathematics, Purdue University, 150 N. University Street, West Lafayette, Indiana 47907-2067

Claudia L. Ravazzoli
Facultad de Ciencias Astronómicas y Geofísicas, Universidad Nacional de La Plata, Paseo del Bosque s/n, 1900 La Plata, Argentina

Hans B. Helle
Norsk Hydro a.s., E & P Research Centre, N-5020 Bergen, Norway

A recent article [J. M. Carcione and G. Seriani, J. Comput. Phys. **170**, 676 (2001)] proposes a modeling algorithm for wave simulation in a three-phase porous medium composed of sand grains, ice, and water. The differential equations hold for uniform water (ice) content. Here, we obtain the variable-porosity differential equations by using the analogy with the two-phase case and the complementary energy theorem. The displacements of the rock and ice frames and the variation of fluid content are the generalized coordinates, and the stress components and fluid pressure are the generalized forces. We simulate wave propagation in a frozen porous medium with fractal variations of porosity and, therefore, realistic freezing conditions. © *2003 American Institute of Physics.*
[DOI: 10.1063/1.1606861]

I. INTRODUCTION

Wave propagation in frozen porous media is a subject which has practical application in many fields, as for instance, seismic prospecting in polar areas (permaforst),[1] evaluation of gas-hydrate concentration in ocean-bottom sediments,[2] and nondestructive evaluation of frozen food by ultrasonic methods.[3,4] These applications require the knowledge of the degree of freezing of the interstitial water. Freezing has a negligible effect on density and magnetic permeability, precluding the use of gravimetric and magnetic techniques, but have a remarkable effect on wave velocities (see Timur,[5] Carcione and Seriani[6]). Hence, seismic and acoustic methods constitute the best way for quantifying the amount of ice and water and determining the degree of freezing.

A Biot-type three-phase theory based on first principles has been proposed by Leclaire *et al.*[7] The theory, which assumes that there is no direct contact between the sand grains and ice, predicts three compressional waves and two shear waves and can be applied to unconsolidated and consolidated porous media. Carcione and Tinivella[2] have generalized the theory to include grain–ice interaction and grain cementation with decreasing temperature, and show an application for the evaluation of gas-hydrate concentration. Carcione and Seriani[8] designed a modeling algorithm based on this new theory. Moreover, they have introduced realistic attenuation by using viscoelastic memory variables, implying additional differential equations.

However, the Lagrangian formulation used by Leclaire *et al.*[7] and, consequently, the differential equations solved by Carcione and Seriani,[8] hold for uniform porosity, since the average displacements of the solid and fluid phases are used as Lagrangian coordinates and the respective stress components are used as generalized forces. These equations are analogous to Biot's 1956 equations describing wave propagation in a two-phase porous medium,[9] which hold for constant porosity. The equations for variable porosity were derived by Biot in 1962,[10] where he proposed the displacements of the matrix and the variation of fluid content as generalized coordinates. In this more general case, the corresponding generalized forces are the total stress components and the fluid pressure. The equations in Ref. 10 are the correct ones for describing wave propagation in an inhomogeneous medium, because they are consistent with Darcy's law and the boundary conditions at interfaces separating media with different properties.

In this article, we obtain the constitutive equations and the equations of momentum conservation of the frozen porous medium by using the analogy with the corresponding two-phase equations of motion, and the complementary energy theorem under small variations of the stresses. The latter approach is illustrated by Santos *et al.*[11] for a partially saturated porous medium and by Biot[10] and Carcione[12] for a saturated porous medium.

[a)]Electronic mail: jcarcione@ogs.trieste.it

7839

II. EQUATIONS OF MOTION

In order to obtain the variable-porosity equations of motion, we proceed by analogy with the two-phase case and use the variation of fluid content and fluid pressure as conjugate variables. Let us indicate by 1, 2, and 3 the field variables related to the rock frame, water, and ice frames, respectively (the subindices "s," "w," and "i" refer to the sand grains, water, and ice particles). Hereafter, the subscripts i and j refer to the spatial variables, and m indicates the constituent. Consider an elementary volume of porous material, where Ω_m are the partial volumes and Ω is the total volume. The amount of ice per unit volume of solid is denoted by I. That is, $I = \Omega_3/(\Omega_1 + \Omega_3)$, and the water proportion is $\phi_w = \Omega_2/\Omega = \Omega_2/(\Omega_1 + \Omega_2 + \Omega_3)$.

The following relations hold

$$\phi_s + \phi_i + \phi_w = 1,$$

$$\phi_w = 1 - \phi_s/(1-I),$$

$$\phi_i = I(1 - \phi_w), \tag{1}$$

where ϕ_s and ϕ_i are the proportions of sand grains and ice. For a given ϕ_s, the range of I is $0 \leq I \leq 1 - \phi_s$. Alternatively, the ice content (or saturation) can be defined as $I' = \Omega_3/(\Omega_2 + \Omega_3)$. Then,

$$\phi_w = (1 - I')(1 - \phi_s),$$

$$\phi_i = I'(1 - \phi_s), \tag{2}$$

with $0 \leq I' \leq 1$. Note that by porosity we mean the water proportion ϕ_w and not the porosity when the rock is completely unfrozen. The latter is the actual rock porosity, given by $\phi_i + \phi_w = 1 - \phi_s$.

A. Conservation of momentum

The equations of momentum conservation for constant porosity can be found in Leclaire *et al.*,[7] Carcione and Tinivella,[2] and Carcione and Seriani.[8] In the last two articles, the interaction between sand grains and ice has been included and, in addition, the stiffening of the rock frame due to grain cementation by ice at freezing temperatures. The three-dimensional equations of momentum conservation can be expressed as

$$\sigma^{(1)}_{ij,j} = \rho_{11}\dot{v}^{(1)}_i + \rho_{12}\dot{v}^{(2)}_i + \rho_{13}\dot{v}^{(3)}_i - b_{12}(v^{(2)}_i - v^{(1)}_i)$$
$$- b_{13}(v^{(3)}_i - v^{(1)}_i),$$

$$\sigma^{(2)}_{,i} = \rho_{12}\dot{v}^{(1)}_i + \rho_{22}\dot{v}^{(2)}_i + \rho_{23}\dot{v}^{(3)}_i + b_{12}(v^{(2)}_i - v^{(1)}_i)$$
$$+ b_{23}(v^{(2)}_i - v^{(3)}_i),$$

$$\sigma^{(3)}_{ij,j} = \rho_{13}\dot{v}^{(1)}_i + \rho_{23}\dot{v}^{(2)}_i + \rho_{33}\dot{v}^{(3)}_i - b_{23}(v^{(2)}_i - v^{(3)}_i)$$
$$+ b_{13}(v^{(3)}_i - v^{(1)}_i), \tag{3}$$

where subscripts $i, j = 1$, 2, and 3 represent the x, y, and z spatial variables, the σ's are macroscopic stress components, the v's are macroscopic particle velocities (per unit volume of porous material), the ρ's are density coefficients, and the

b's are friction coefficients. A dot above a variable denotes time differentiation and spatial derivatives with respect to a variable x_i is indicated by the subscript "i."

The friction terms in Eq. (3) have the opposite sign of those given in Ref. 7, otherwise the equations are physically unstable (wave amplitude increases with time). The signs here coincide with those of Biot's differential equations[10,12] in the limit of full water saturation. Expressions of the physical quantities are given in Appendix A, and their physical meaning is explained in Carcione and Tinivella[2] and Carcione and Seriani.[6,8]

The analysis in Appendix B shows that the relative displacement of the fluid relative to the rock and ice frames (taken as a composite) is

$$w_i = \phi_w[u^{(2)}_i - (1-I)u^{(1)}_i - Iu^{(3)}_i], \tag{4}$$

where the u's denote the macroscopic displacements ($v = \dot{u}$), ϕ_w is the proportion of water, and I is the ice content (see Appendix A). Alternatively, we can define

$$w_i = (1-I)w^{(1)}_i + Iw^{(3)}_i, \tag{5}$$

where

$$w^{(1)}_i = \phi_w(u^{(2)}_i - u^{(1)}_i)$$
$$w^{(3)}_i = \phi_w(u^{(2)}_i - u^{(3)}_i) \tag{6}$$

are the familiar two-phase relative displacements.[10]

Substituting Eq. (4) into (3) and using the expressions given in Appendix A, we obtain for the solid phases:

$$\sigma^{(1)}_{ij,j} = [\rho_{11} + (1-I)\rho_{12}]\dot{v}^{(1)}_i + (\rho_{13} + I\rho_{12})\dot{v}^{(3)}_i$$
$$+ (\rho_{12}/\phi_w)\ddot{w}_i + (b_{13} + Ib_{12})(v^{(1)}_i - v^{(3)}_i)$$
$$- (b_{12}/\phi_w)\dot{w}_i, \tag{7}$$

and

$$\sigma^{(3)}_{ij,j} = [\rho_{13} + (1-I)\rho_{23}]\dot{v}^{(1)}_i + (\rho_{33} + I\rho_{23})\dot{v}^{(3)}_i$$
$$+ (\rho_{23}/\phi_w)\ddot{w}_i - [b_{13} + (1-I)b_{23}](v^{(1)}_i - v^{(3)}_i)$$
$$- (b_{23}/\phi_w)\dot{w}_i. \tag{8}$$

On the other hand, the second Eq. (3) can be rewritten as

$$-p_{f,i} = \rho_{w1}\dot{v}^{(1)}_i + \rho_{w3}\dot{v}^{(3)}_i + m\ddot{w}_i + \left(\frac{\eta_w}{\kappa_s}\right)\dot{w}^{(1)}_i$$
$$+ \left(\frac{\eta_w}{\kappa_i}\right)\dot{w}^{(3)}_i, \tag{9}$$

where κ_s and κ_i are the rock- and ice-frame permeabilities, and η_w is the viscosity of water. Alternatively, Eq. (9) can be expressed as

$$-p_{f,i} = \rho_{w1}\dot{v}^{(1)}_i + \rho_{w3}\dot{v}^{(3)}_i + m\ddot{w}_i$$
$$+ \left(\frac{\eta_w}{\kappa}\right)\left[\dot{w}_i + \phi_w\left(I - \frac{\kappa}{\kappa_i}\right)(v^{(3)}_i - v^{(1)}_i)\right], \tag{10}$$

where p_f is the fluid pressure, satisfying

$$\sigma^{(2)} = -\phi_w p_f, \tag{11}$$

$$\rho_{w1} = \rho_w[I(1-a_{21})+a_{23}(1-I)],$$

$$\rho_{w3} = \rho_w - \rho_{w1},$$

$$m = \rho_w(a_{21}+a_{23}-1)/\phi_w, \tag{12}$$

and

$$\kappa = \frac{\kappa_s \kappa_i}{\kappa_s + \kappa_i}, \tag{13}$$

is the effective permeability.

Defining the total stress as

$$\sigma_{ij} = \sigma_{ij}^{(1)} + \sigma_{ij}^{(3)} - \phi_w p_f \delta_{ij}, \tag{14}$$

its divergence can be obtained by using Eqs. (7), (8), (10), and (11). It gives

$$\sigma_{ij,j} = (1-I)[(1-\phi_w)\rho_s + \rho_w\phi_w]\dot{v}_i^{(1)}$$

$$+ I[(1-\phi_w)\rho_i + \rho_w\phi_w]\dot{v}_i^{(3)} + \rho_w \ddot{w}_i. \tag{15}$$

In the case that the two frames move in phase and their properties are similar, we have $v_i^{(3)} = v_i^{(1)}$, and Eqs. (10) and (15) reduce to the equations of motion of the two-phase case (see, for instance, Biot[10] and Eqs. (7.210) and (7.211) in Carcione[12]).

B. Stress–strain relations

The three-dimensional stress–strain relations for constant porosity are given by[2,8]

$$\sigma_{ij}^{(1)} = (K_1\theta_1 + C_{12}\theta_2 + C_{13}\theta_3)\delta_{ij} + 2\mu_1 d_{ij}^{(1)} + \mu_{13}d_{ij}^{(3)},$$

$$\sigma^{(2)} = C_{12}\theta_1 + K_2\theta_2 + C_{23}\theta_3,$$

$$\sigma_{ij}^{(3)} = (K_3\theta_3 + C_{23}\theta_2 + C_{13}\theta_1)\delta_{ij} + 2\mu_3 d_{ij}^{(3)} + \mu_{13}d_{ij}^{(1)}, \tag{16}$$

where K, C, and μ are moduli whose expressions are given in Appendix A:

$$\theta_m = \epsilon_{ii}^{(m)},$$

$$d_{ij}^{(m)} = \epsilon_{ij}^{(m)} - \tfrac{1}{3}\delta_{ij}\theta_m,$$

$$\epsilon_{ij}^{(m)} = \tfrac{1}{2}(u_{i,j}^{(m)} + u_{j,i}^{(m)}), \quad m=1,3, \tag{17}$$

are the dilatations, deviatoric components of strain and strain components, respectively (implicit summation over the repeated index i is assumed), and δ_{ij} represents Kronecker's delta.

The constitutive equations corresponding to the two-dimensional case are obtained by removing one of the dimensions (say, the y dimension), and replacing the coefficients $K_1 + 4\mu_1/3$ and $K_1 - 2\mu_1/3$ by $K_1 + \mu_1$ and $K_1 - \mu_1$, respectively (which appear when the equations are rewritten in terms of the strain components[8]). Similarly, $C_{13} + 2\mu_{13}/3$ and $C_{13} - \mu_{13}/3$ are to be replaced by $C_{13} + \mu_{13}/2$ and $C_{13} - \mu_{13}/2$, respectively.

We introduce the variation of fluid content as the divergence of the relative displacement vector defined in Eq. (4):

$$\zeta = -\text{div } \mathbf{w} = -\{\phi_w[u_i^{(2)} - (1-I)u_i^{(1)} - Iu_i^{(3)}]\}_{,i}, \tag{18}$$

which, for constant porosity, becomes

$$\zeta = -\phi_w[\theta_2 - (1-I)\theta_1 - I\theta_3]. \tag{19}$$

Substituting θ_2 by $(1-I)\theta_1 + I\theta_3 - \zeta/\phi_w$ into Eq. (16) yields

$$\sigma_{ij}^{(1)} = [(K_{G1} - \alpha_1 M(1-I)\phi_w)\theta_1 + M(\alpha_1 - (1-I)\phi_w)$$

$$\times (\alpha_3\theta_3 - \zeta)]\delta_{ij} + 2\mu_1 d_{ij}^{(1)} + \mu_{13}d_{ij}^{(3)},$$

$$p_f = M(\zeta - \alpha_1\theta_1 - \alpha_3\theta_3),$$

$$\sigma_{ij}^{(3)} = [(K_{G3} - \alpha_3 MI\phi_w)\theta_3 + M(\alpha_3 - I\phi_w)(\alpha_1\theta_1$$

$$- \zeta)]\delta_{ij} + 2\mu_3 d_{ij}^{(3)} + \mu_{13}d_{ij}^{(1)}, \tag{20}$$

where

$$K_{G1} = K_{sm} + \alpha_1^2 M,$$

$$K_{G3} = K_{im} + \alpha_3^2 M,$$

$$M = K_2/\phi_w^2 = K_{av},$$

$$\alpha_1 = 1 - K_{sm}/K_s - I,$$

$$\alpha_3 = 1 - K_{im}/K_i - (1-I). \tag{21}$$

The total stress (14) is then given by

$$\sigma_{ij} = [(K_{G1} + \alpha_1\alpha_3 M)\theta_1 + (K_{G3} + \alpha_1\alpha_3 M)\theta_3 - M(\alpha_1$$

$$+ \alpha_3)\zeta]\delta_{ij} + (2\mu_1 + \mu_{13})d_{ij}^{(1)} + (2\mu_3 + \mu_{13})d_{ij}^{(3)}. \tag{22}$$

The analogy between these equations and those corresponding to a two-phase porous medium is evident. The second Eq. (20) and Eq. (22) correspond to Eqs. (7.32) and (7.33) of Carcione,[12] the K_{Gm}, $m=1$ and 3 are analogous to Gassmann's modulus, and the α_m are analogous to the effective stress coefficients predicted by Biot theory.[10,12]

If we consider the isostrain state, $\theta_1 = \theta_2 = \theta_3$, $\zeta = 0$ and we have the conditions of a "closed system." In this case, the bulk modulus is

$$K_G = K_{sm} + K_{im} + \alpha^2 M, \tag{23}$$

where

$$\alpha = \alpha_1 + \alpha_3 = 1 - K_{sm}/K_s - K_{im}/K_i. \tag{24}$$

The modulus K_G is a generalization of the Gassmann (low frequency) modulus of the classical Biot theory.[13]

Equations (7), (8), (10), and (20) constitute the equations of motion of the three-phase porous medium valid for variable porosity, since they are expressed in terms of the stress components of the solid phases, fluid pressure, and variation of fluid content. A justification that these are the correct generalized coordinates, based on the complementary energy theorem is given in Sec. III.

III. STRAIN ENERGY

The variation in strain energy for small variations of the stresses is obtained in Appendix B. (The approach is based on the complementary energy theorem.) It is given by

$$\delta V = (1-I)\,\delta(\tau_{ij}^{(1)} - \phi_w p_f \delta_{ij})\epsilon_{ij}^{(1)} + I\,\delta(\tau_{ij}^{(3)}$$
$$- \phi_w p_f \delta_{ij})\epsilon_{ij}^{(3)} + \delta p_f \zeta, \tag{25}$$

where $\tau_{ij}^{(m)}$ are the average stress components per unit volume of solid (grains plus ice). Since the properties in the elementary Ω are constant (although they may vary point to point in the porous medium), we can express [on the basis of Eq. (25)] the strain energy as[12]

$$2V = [\sigma_{ij}^{(1)} - (1-I)\phi_w p_f \delta_{ij}]\epsilon_{ij}^{(1)}$$
$$+ (\sigma_{ij}^{(3)} - I\phi_w p_f \delta_{ij})\epsilon_{ij}^{(3)} + p_f \zeta, \tag{26}$$

and

$$\sigma_{ij}^{(1)} = \frac{\partial V}{\partial \epsilon_{ij}^{(1)}} + (1-I)\phi_w p_f \delta_{ij},$$

$$\sigma_{ij}^{(3)} = \frac{\partial V}{\partial \epsilon_{ij}^{(3)}} + I\phi_w p_f \delta_{ij}, \quad p_f = \frac{\partial V}{\partial \zeta}, \tag{27}$$

where we have used the relation $\sigma_{ij}^{(m)} = \phi_m \tau_{ij}^{(m)}$, with $\phi_1 = 1-I$ and $\phi_3 = I$. The two-phase strain energy[10,12] is obtained when the two solids move in phase ($\epsilon_{ij}^{(1)} = \epsilon_{ij}^{(3)}$), since $\sigma_{ij}^{(1)} - \phi_w p_f \delta_{ij}$ equals the total stress.

It is clear from Eq. (27) that the generalized coordinates regard the strain components $\epsilon_{ij}^{(1)}$, $\epsilon_{ij}^{(3)}$, and ζ, and the corresponding generalized forces are $\sigma_{ij}^{(1)} - (1-I)\phi_w p_f \delta_{ij}$ and $\sigma_{ij}^{(3)} - I\phi_w p_f \delta_{ij}$, and the fluid pressure p_f. Use of the variation of fluid content instead of the fluid displacement is consistent with Darcy's law and the boundary conditions at interfaces separating dissimilar media.[12]

A more rigorous demonstration of the validity of the variable-porosity formulation obtained here is given in another work,[14] where the equations of motion are obtained by using the virtual work principle based on small variations of the displacements and Lagrange's equations. A theorem on the existence, uniqueness, and regularity of the solution of the equations of motion under appropriate initial and boundary conditions is also given.

IV. VELOCITY-STRESS FORMULATION

The numerical algorithm requires to recast the equation of motion in the velocity-stress formulation.[8] The velocity-stress formulation are first-order differential equations (in the space and time variables), where the unknown variables are the particle velocities and stress components. The equations of momentum conservation can then be rewritten by using Eqs. (7), (8), and (10) as

$$\dot{v}_i^{(1)} = \gamma_{11}\Pi_i^{(1)} + \gamma_{12}\Pi_i^{(2)} + \gamma_{13}\Pi_i^{(3)},$$

$$\dot{v}_i^{(3)} = \gamma_{21}\Pi_i^{(1)} + \gamma_{22}\Pi_i^{(2)} + \gamma_{23}\Pi_i^{(3)},$$

$$\dot{w}_i = \gamma_{31}\Pi_i^{(1)} + \gamma_{32}\Pi_i^{(2)} + \gamma_{33}\Pi_i^{(3)}, \tag{28}$$

where

$$\Pi_i^{(1)} = \sigma_{ij,j}^{(1)} - (b_{13} + Ib_{12})(v_i^{(1)} - v_i^{(3)}) + (b_{12}/\phi_w)\dot{w}_i,$$

$$\Pi_i^{(2)} = \sigma_{ij,j}^{(3)} + [b_{13} + (1-I)b_{23}](v_i^{(1)} - v_i^{(3)})$$
$$+ (b_{23}/\phi_w)\dot{w}_i,$$

$$\Pi_i^{(3)} = -p_{f,i} - (\eta_w/\kappa)[\dot{w}_i + \phi_w(I - \kappa/\kappa_i)(v_i^{(3)} - v_i^{(1)})], \tag{29}$$

and γ_{nm} are the components of the following matrix

$$\begin{pmatrix} \rho_{11} + (1-I)\rho_{12} & \rho_{13} + I\rho_{12} & \rho_{12}/\phi_w \\ \rho_{13} + (1-I)\rho_{23} & \rho_{33} + I\rho_{23} & \rho_{23}/\phi_w \\ \rho_{w1} & \rho_{w3} & m \end{pmatrix}^{-1}. \tag{30}$$

The equations for the stress components are obtained by differentiating Eqs. (20) with respect to the time variable, and using the relations $\dot{\epsilon}_{ij}^{(m)} = (v_{i,j}^{(m)} + v_{j,i}^{(m)})/2$, $m = 1$ and 3.

The velocity-stress differential equations can be written in matrix form as

$$\dot{\mathbf{v}} = \mathbf{M}\mathbf{v} + \mathbf{s}, \tag{31}$$

where

$$\mathbf{v} = [v_i^{(1)}, v_i^{(3)}, \dot{w}_i, \sigma_{ij}^{(1)}, \sigma_{ij}^{(3)}, p_f]^\top, \tag{32}$$

is the unknown velocity-stress vector of dimension 22 in 3D space and dimension 13 in 2D space

$$\mathbf{s} = [0,0,0,0,0,0,0,0,0, \ s_{ij}^{(1)}, s_{ij}^{(3)}, s^{(2)}]^\top \tag{33}$$

is the source vector (3D space), and $\mathbf{M}$ is the propagation matrix containing the spatial derivatives and material properties. (Sources are added to the stress components and fluid pressure.)

V. NUMERICAL ALGORITHM

The solution to Eq. (31) subject to the initial condition $\mathbf{v}(0) = \mathbf{v}_0$ is formally given by

$$\mathbf{v}(t) = \exp(t\mathbf{M})\mathbf{v}_0 + \int_0^t \exp(\tau\mathbf{M})s(t-\tau)d\tau, \tag{34}$$

where $\exp(t\mathbf{M})$ is called evolution operator.

As in the constant porosity case,[8] the eigenvalues of $\mathbf{M}$ have negative real parts and differ greatly in magnitude due to the viscosity terms. The presence of large eigenvalues, together with small eigenvalues, indicates that the problem is stiff. The differential equations are solved with the splitting algorithm used by Carcione and Seriani.[8] The propagation matrix can be partitioned as

$$\mathbf{M} = \mathbf{M}_r + \mathbf{M}_s, \tag{35}$$

where subscript r indicates the regular matrix, and subscript s the stiff matrix. We discretize the time variable as $t = ndt$, where dt is the time step. The evolution operator can be expressed as $\exp(\mathbf{M}_r + \mathbf{M}_s)t$. It is easy to show that the product formula

$$\exp(\mathbf{M}dt) = \exp(\tfrac{1}{2}\mathbf{M}_s dt)\exp(\mathbf{M}_r dt)\exp(\tfrac{1}{2}\mathbf{M}_s dt) \tag{36}$$

J. Appl. Phys., Vol. 94, No. 12, 15 December 2003

Carcione *et al.* 7843

is second-order accurate in dt. Equation (36) allow us to solve the stiff part separately. Using the Kronecker product "$\otimes$" of two matrices, the stiff matrix in two-dimensional space can be expressed as

$$\mathbf{M}_s = \begin{pmatrix} \mathbf{I}_2 \otimes \mathbf{S} & \mathbf{0} \\ \mathbf{0} & \mathbf{0} \end{pmatrix}, \tag{37}$$

where $\mathbf{I}_2$ is the 2×2 identity matrix. We should solve

$$\dot{\mathbf{w}}_i = \mathbf{S}\mathbf{w_i}, \tag{38}$$

for each Cartesian component i, where

$$\mathbf{w}_i = [v_i^{(1)}, v_i^{(3)}, w_i]^\top, \tag{39}$$

and the components of $\mathbf{S}$ are

$$\mathbf{S}_{11} = a\gamma_{11} + c\gamma_{12} + [Ib - (1-I)d]\gamma_{13},$$

$$\mathbf{S}_{12} = -\mathbf{S}_{11},$$

$$\mathbf{S}_{13} = b\gamma_{11} + d\gamma_{12} - [(b+d)/\phi_w]\gamma_{13},$$

$$\mathbf{S}_{21} = a\gamma_{21} + c\gamma_{22} + [Ib - (1-I)d]\gamma_{23},$$

$$\mathbf{S}_{22} = -\mathbf{S}_{21},$$

$$\mathbf{S}_{23} = b\gamma_{21} + d\gamma_{22} - [(b+d)/\phi_w]\gamma_{23},$$

$$\mathbf{S}_{31} = a\gamma_{31} + c\gamma_{32} + [Ib - (1-I)d]\gamma_{33},$$

$$\mathbf{S}_{32} = -\mathbf{S}_{31},$$

$$\mathbf{S}_{33} = b\gamma_{31} + d\gamma_{32} - [(b+d)/\phi_w]\gamma_{33}, \tag{40}$$

where

$$a = -(b_{13} + Ib_{12}), \quad b = b_{12}/\phi_w,$$

$$c = b_{13} + (1-I)b_{23}, \quad d = b_{23}/\phi_w. \tag{41}$$

Since matrix $\mathbf{S}$ has two linearly dependent columns, one of its eigenvalues is zero. The other two eigenvalues are

$$\lambda_1 = \tfrac{1}{2}[\mathrm{tr}(\mathbf{S}) - \sqrt{4(\mathbf{S}_{13} - \mathbf{S}_{23})\mathbf{S}_{31} + (\mathbf{S}_{21} + \mathbf{S}_{33} - \mathbf{S}_{11})^2}],$$

$$\lambda_2 = \mathrm{tr}(\mathbf{S}) - \lambda_1. \tag{42}$$

The solution of the vector differential Eq. (38), with this condition, is given in Carcione and Seriani.[8]

The time stepping method is a Runge–Kutta fourth-order algorithm, and the spatial derivatives are calculated with the Fourier method by using the FFT.[12] This spatial approximation is infinitely accurate for band-limited periodic functions with cutoff spatial wave numbers which are smaller than the cutoff wave numbers of the mesh. Due to the splitting algorithm, the modeling is second-order accurate in the time discretization. The method is illustrated in detail in Carcione and Helle[15] for a two-phase medium and in Carcione and Seriani[8] for a three-phase medium.

VI. EXAMPLE

To illustrate the use of the variable-porosity differential equations, we consider wave propagation in a frozen sandstone with an average (real) porosity of 20% when the medium is unfrozen ($1 - \phi_s = 0.2$). The data (see Table I) correspond to Berea sandstone, with the properties given by

TABLE I. Material properties for frozen Berea sandstone.

Media	Density (kg/m^3)	Bulk modulus (GPa)	Shear modulus (GPa)
Grain	$\rho_s = 2650$	$K_s = 38.7$	$\mu_s = 39.6$
Ice	$\rho_i = 920$	$K_i = 8.58$	$\mu_i = 3.32$
Water	$\rho_w = 1000$	$K_w = 2.25$	$\mu_w = 0$

Timur[5] and Winkler.[16] The dry-rock bulk and shear moduli are $K_{sm} = 14.4$ GPa and $\mu_{sm0} = 13.1$ GPa; the rock-frame and ice-frame permeabilities are $\kappa_{s0} = 1.07 \times 10^{-13}$ and $\kappa_{i0} = 5 \times 10^{-4}$ m^2; and the fluid viscosity is $\eta_w = 1.8$ cP (1 cP $= 0.001$ Pa s). We assume $a_{13} = a_{31} = 1$ and no friction between the rock and ice frames ($b_{13} = 0$).

Figure 1 shows the phase velocities of the five wave modes versus water proportion, where the compressional waves are labeled P1, P2, and P3, and the shear waves are labeled S1 and S2. The velocities at different freezing conditions are indicated. At full water saturation ($\phi_w = 0.2$, $I = 0$) three waves propagate, and the velocities are those predicted by Biot's theory.

We consider a 357×357 mesh, with square cells and a grid spacing of 0.84 mm (the sample has a dimension of 30×30 cm). Fractal variations of porosity (water content) are computed as described in Appendix C. The case $\phi_w = 0.1$ (50% water saturation) and $\Delta\phi = 0.1$ is shown in Fig. 2. This model includes regions of full water and ice saturation.

Let us consider an ultrasound experiment, where the source pulse has a dominant frequency of 500 kHz and consists of bulk sources and shear forces in the rock frame and ice matrix and a fluid-volume injection in the fluid. Snapshots of the wavefield ($v_z^{(1)}$ component of the sand grain and ice frames), corresponding to $\phi_w = 0.1$ ($I = 0.5$), (a) $\Delta\phi = 0$ and (b) $\Delta\phi = 0.1$, are shown in Figs. 3(a) and 3(b), respectively. The average size of the heterogeneities is $a = 1$ mm
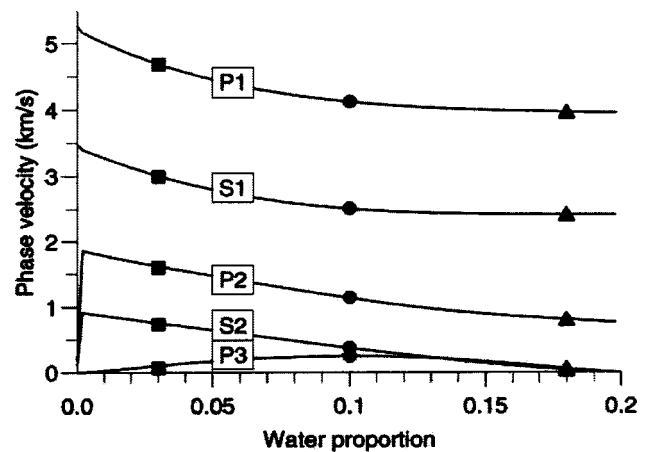

FIG. 1. Phase velocities of the five wave modes propagating in partially frozen Berea sandstone vs water proportion. The compressional waves are labeled P1, P2, and P3, and the shear waves are labeled S1 and S2. The squares, circles, and triangles indicate the velocities at 15%, 50%, and 90% water saturation, where the values of the velocities are 4713, 4122, and 3962 m/s for P1; 3024, 2480, and 2408 m/s for S1; 1637, 1142, and 808 m/s for P2; 767, 380, and 39 m/s for S2 and 100; 250 and 60 m/s for P3, respectively.
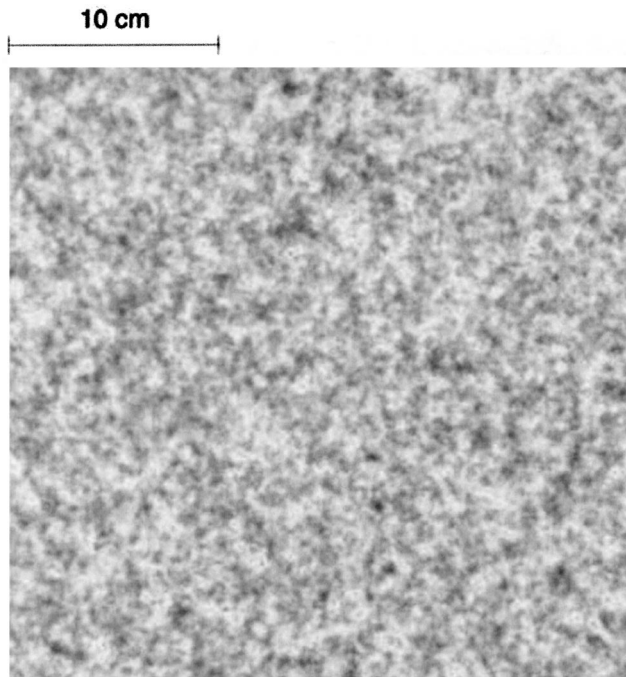
FIG. 2. Water-proportion fractal variations obtained from the von Kármán autocovariance function: ($\nu=0.15$, $a=1$ mm, $\phi_w=0.1$, and $\Delta\phi=0.1$; see Appendix C).

FIG. 4. Time histories corresponding to $\phi_w=0.1$, $\Delta\phi=0$ (solid line), $\Delta\phi=0.05$ (dashed line), and $\Delta\phi=0.1$ (dotted line). The source-receiver distance is 6 cm. The source-receiver line makes an angle of 30° with the vertical direction.

($\eta\neq0$), the slow modes are weaker but are still propagating modes, as can be deduced from the phase velocities shown in Fig. 1. The energy of the slow waves P2, S2, and P3 propagate mainly in the ice frame. Besides scattering, mode conversion occurs at heterogeneities.

The nature of the different wave modes is the following: (i) P1 and S1 are the usual waves which we observe in acoustics of material media. They correspond to all the phases moving in phase, and propagate irrespective of the value of the viscosity and permeabilities; (ii) P2 is the Biot wave. It is a propagation mode for full water saturation and $b_{12}=0$ (the case in Fig. 3, i.e., zero viscosity or infinite rock-frame permeability) and a quasistatic mode for full water saturation and $b_{12}\neq0$ (assuming realistic values of viscosity and permeability); (iii) P2 and S2 are propagation modes in the presence of ice (excluding $\phi_w=0$, as previously mentioned). These modes become waves with increasing freezing and are strong in the ice frame, as predicted by the images in Fig. 3. (iv) P3 is quasistatic at zero and full water saturations, even in the absence of friction between the phases. This wave could probably be observed in synthetic partially frozen materials and under very particular conditions, e.g., a fluid of negligible viscosity (obviously not water) and a highly permeable porous medium. (v) The condition of no slow-wave motion in the solid/solid case [the case of a totally frozen medium ($\phi_w=0$) (see Fig. 1)] is found for very low water saturation (the velocities of P3 and S2 vanish at $\phi_w=0$).

Figure 4 shows time histories of the particle-velocity component $v_z^{(1)}$ (sand-grain frame) for $\phi_w=0.1$ ($I=0.5$), $\Delta\phi=0$ (solid line), $\Delta\phi=0.05$ (dashed line) and $\Delta\phi=0.1$ (dotted line). In this case the viscosity is $\eta_w=1.8$ cP. The amplitude of the P1 wave (pulse at 15 μs) is not affected, but that of the S1 wave (pulse at 23 μs) increases with increasing degree of heterogeneity (increasing $\Delta\phi$).

Time histories of $v_z^{(1)}$ (sand-grain frame) for different freezing conditions are shown in Fig. 5. They correspond to $\phi_w=0.1$ ($I=0.5$) (solid line), $\phi_w=0.03$ ($I=0.9$) (dashed line), and $\phi_w=0.18$ ($I=0.15$) (dotted line), with $\Delta\phi=0.02$ in all the cases. The pulses are the P1 and S1 waves, whose velocities are given in Fig. 1. The time histories indicate that, as expected, the waves are slower for increasing water content.

(see Appendix C). The ratio maximum amplitude in $v_z^{(1)}$ (sand) (a) to maximum amplitude in $v_z^{(3)}$ (ice) (a) is 26. The ratio is 62 for the snapshots in Fig. 3(b). (Waves S2 and P3 are aliased, since the mesh "supports" a minimum velocity of 960 m/s according to the Nyquist criterion.) We have considered an ideal fluid ($\eta_w=0$) in order to appreciate the scattering effects in the slow modes also. For a real fluid

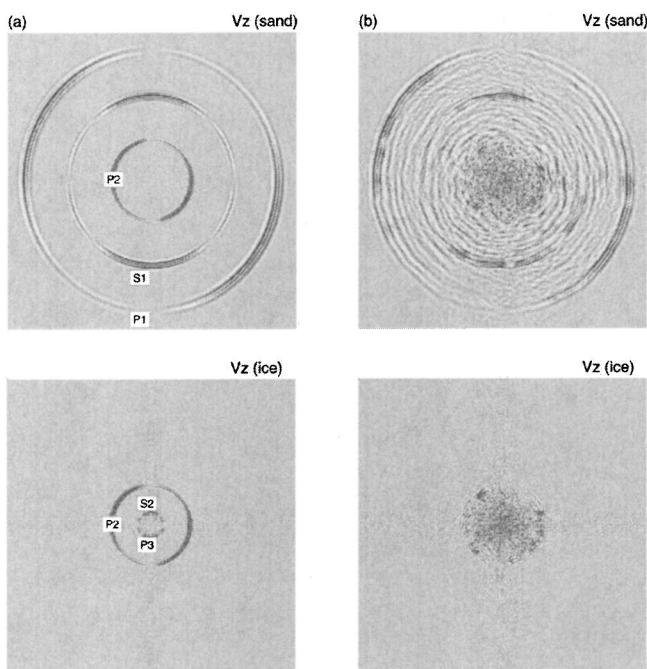FIG. 3. Snapshots of the rock-frame particle-velocity component v_z at 37 μs, corresponding to $\phi_w=0.1$, (a) $\Delta\phi=0$ (homogeneous medium) and (b) $\Delta\phi=0.1$. The mesh has 357×357 grid points and the source is applied at grid point (178, 178). The compressional waves are labeled P1, P2, and P3, and the shear waves are labeled S1 and S2.
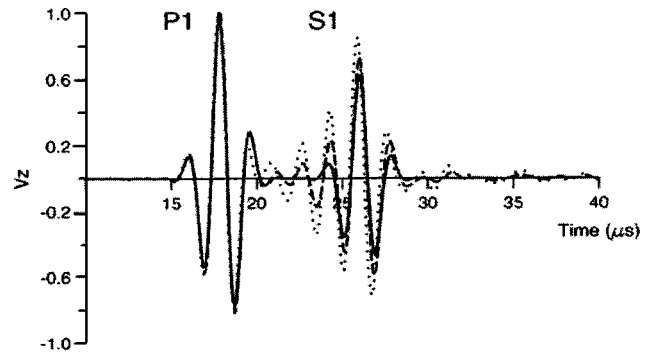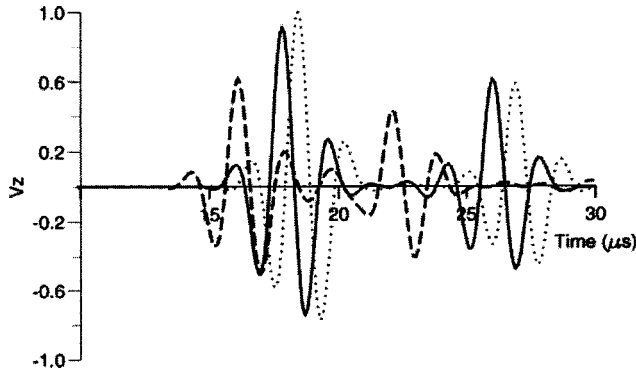
FIG. 5. Time histories corresponding to $\phi_w = 0.1$ (solid line), $\phi_w = 0.03$ (dashed line), and $\phi_w = 0.18$ (dotted line), with $\Delta\phi = 0.02$ in all the cases. The source-receiver distance is 6 cm. The source-receiver line makes an angle of 30° with the vertical direction. The pulses correspond to the P1 and S1 waves (see velocities in Fig. 1).

VII. CONCLUSIONS

We have developed a numerical algorithm for wave simulation in a frozen porous medium with nonuniform water content. The differential equations are based on a three-phase Biot-type theory. The algorithm, which is second-order accurate in time and has spectral accuracy in the space variable, allows general material variability and provides snapshots and time histories of the rock frame, ice matrix, and water particle velocities and corresponding stress components.

In the process of freezing two major events are the formation of ice crystals (nucleation) and the subsequent increase in size of these crystals. In rocks, this process occurs first in the larger pores (due to surface-tension effects). Hence, the degree of freezing is not spatially uniform. The example shows how to model realistic freezing conditions with a fractal distribution of the water (or ice) content. The modeling algorithm can be used to predict ultrasonic velocities and attenuation for frozen porous media. (Attenuation can easily be incorporated by using a viscoelastic stress–strain relation.)

APPENDIX A: EXPRESSIONS OF THE THEORY

The following expressions correspond to the theory of wave propagation in three-phase porous media,[2,6,7,8] where 1, 2, and 3 denote quantities related to the sand grains, water, and ice, respectively.

The friction coefficients are

$$b_{12} = \eta_w \phi_w^2 / \kappa_s,$$

$$b_{23} = \eta_w \phi_w^2 / \kappa_i,$$

where η_w and ϕ_w are the viscosity and proportion of water, and κ_s and κ_i are the rock- and ice-frame permeabilities (see below). The consolidation coefficients of the rock and ice frames are

$$c_1 = K_{sm} / \phi_s K_s,$$

$$c_3 = K_{im} / \phi_i K_i,$$

where ϕ_s, ϕ_i and K_s, K_i are the proportions and bulk moduli of the sand grains and ice, respectively, K_{sm} is the bulk modulus of the rock frame, and

$$K_{im} = K_{\max}[\phi_i / (1 - \phi_s)]^{3.8}$$

is the bulk modulus of the ice frame, where $K_{\max}$ is Kuster–Toksöz's bulk modulus of the ice matrix.

The off-diagonal coupling moduli are

$$C_{12} = (1 - c_1) \phi_s \phi_w K_{av},$$

$$C_{13} = (1 - c_1)(1 - c_3) \phi_s \phi_i K_{av},$$

$$C_{23} = (1 - c_3) \phi_i \phi_w K_{av},$$

where

$$K_{av} = [(1 - c_1) \phi_s / K_s + \phi_w / K_w + (1 - c_3) \phi_i / K_i]^{-1},$$

is the average bulk modulus and K_w is the bulk modulus of water.

The ice content can be expressed as

$$I = \phi_i / (\phi_s + \phi_i).$$

The diagonal coupling moduli are

$$K_1 = [(1 - c_1) \phi_s]^2 K_{av} + K_{sm},$$

$$K_2 = \phi_w^2 K_{av},$$

$$K_3 = [(1 - c_3) \phi_i]^2 K_{av} + K_{im}.$$

The permeabilities of the rock and ice frames are

$$\kappa_s = \kappa_{s0} \phi_w^3 / (1 - \phi_s)^3,$$

$$\kappa_i = \kappa_{i0}[(1 - \phi_s) / \phi_i]^2 (\phi_w / \phi_s)^3,$$

where κ_{s0} and κ_{i0} are reference values.

The components of the rigidity matrix are

$$\mu_1 = [(1 - g_1) \phi_s]^2 \mu_{av} + \mu_{sm},$$

$$\mu_{13} = (1 - g_1)(1 - g_3) \phi_s \phi_i \mu_{av},$$

$$\mu_3 = [(1 - g_3) \phi_i]^2 \mu_{av} + \mu_{im},$$

where

$$\mu_{sm} = [\mu_{sm\mathrm{KT}} - \mu_{sm0}][\phi_i / (1 - \phi_s)]^{3.8} + \mu_{sm0},$$

is the shear modulus of the rock frame, $\mu_{sm\mathrm{KT}}$ is the Kuster–Toksöz shear modulus of the rock frame, μ_{sm0} is the shear modulus of the rock frame at full water saturation,

$$\mu_{im} = \mu_{\max}[\phi_i / (1 - \phi_s)]^{3.8}$$

is the shear modulus of the ice frame, $\mu_{\max}$ is Kuster–Toksöz's shear modulus of the ice frame, and

$$\mu_{av} = [(1 - g_1) \phi_s / \mu_s + \phi_w / i\omega \eta_w + (1 - g_3) \phi_i / \mu_i]^{-1},$$

is the average shear modulus, with ω being the angular frequency, and μ_s and μ_i being the shear moduli of the sand grains and ice, respectively.

The consolidation coefficients of the rock and ice frames are

$$g_1 = \mu_{sm}/\phi_s \mu_s,$$

$$g_3 = \mu_{im}/\phi_i \mu_i.$$

The components of the density matrix are

$$\rho_{11} = \phi_s \rho_s a_{13} + (a_{21}-1)\phi_w \rho_w + (a_{31}-1)\phi_i \rho_i,$$

$$\rho_{12} = -(a_{21}-1)\phi_w \rho_w,$$

$$\rho_{13} = -(a_{13}-1)\phi_s \rho_s - (a_{31}-1)\phi_i \rho_i,$$

$$\rho_{22} = (a_{21}+a_{23}-1)\phi_w \rho_w,$$

$$\rho_{23} = -(a_{23}-1)\phi_w \rho_w,$$

$$\rho_{33} = \phi_i \rho_i a_{31} + (a_{23}-1)\phi_w \rho_w + (a_{13}-1)\phi_s \rho_s,$$

where ρ_s, ρ_i, and ρ_w are the density of the sand grains, ice, and water, respectively.

We express the tortuosities as:[7]

$$a_{21} = \left(\frac{\phi_s \rho}{\phi_w \rho_w}\right)r_{21}+1, \quad a_{23} = \left(\frac{\phi_i \rho'}{\phi_w \rho_w}\right)r_{23}+1, \tag{A1}$$

where

$$\rho = \frac{\phi_w \rho_w + \phi_i \rho_i}{\phi_w + \phi_i}, \quad \rho' = \frac{\phi_w \rho_w + \phi_s \rho_s}{\phi_w + \phi_s},$$

and r_{21} and r_{23} characterize the geometrical features of the pores (1/2 for spheres). By analogy, we consider that

$$a_{13} = \left(\frac{\phi_i \rho''}{\phi_s \rho_s}\right)r_{13}+1, \quad a_{31} = \left(\frac{\phi_s \rho''}{\phi_i \rho_i}\right)r_{31}+1, \tag{A2}$$

where

$$\rho'' = \frac{\phi_i \rho_i + \phi_s \rho_s}{\phi_i + \phi_s}.$$

Equation (A2) should be used with caution, and it is convenient in most of the cases to use a_{13} and a_{31} as free parameters, as well as the friction coefficient b_{13} between the sand grains and the ice.

APPENDIX B: STRAIN ENERGY

First, let us clarify the meaning of the different averaged stress tensor components. Assume that $m=1$ and 3 refers to the solid components (sand grains and ice, respectively), and define $s_{ij}^{(m)}$ as the average values of the stress tensor over Ω_m. Then, the contributions of the solid phases to the total stress tensor are $\sigma_{ij}^{(1)} = \phi_s s_{ij}^{(1)} = (1-I)(1-\phi_w)s_{ij}^{(1)}$ and $\sigma_{ij}^{(3)} = \phi_i s_{ij}^{(3)} = I(1-\phi_w)s_{ij}^{(3)}$, according to Eqs. (1) and (14). We introduce the averaged components per unit volume of solid (grains plus ice), $\tau_{ij}^{(1)}$, through the relations $\sigma_{ij}^{(1)} = (1-I)\tau_{ij}^{(1)}$ and $\sigma_{ij}^{(3)} = I\tau_{ij}^{(3)}$.

The approach to evaluate the variation of strain energy, and, therefore, the generalized coordinates and corresponding conjugate variables, follows the development given by Biot[10] and Carcione[12] for a two-phase porous medium. Let us consider a volume Ω of porous material bounded by the surface S. Assume that Ω is initially in static equilibrium under the action of the surface forces—per unit volume of bulk material acting on the three phases. These forces can be written as

$$f_i^{(1)} = \sigma_{ij}^{(1)}n_j = (1-I)\tau_{ij}^{(1)}n_j,$$

$$f_i^{(2)} = -\phi_w p_f \delta_{ij}n_j,$$

$$f_i^{(3)} = \sigma_{ij}^{(3)}n_j = I\tau_{ij}^{(3)}n_j, \tag{B1}$$

where n_j are the components of the outward unit vector perpendicular to S. Assume that the system is perturbed by $\delta f_i^{(1)}$, $\delta f_i^{(2)}$, and $\delta f_i^{(3)}$, and let $V(\delta f_i^{(1)}, \delta f_i^{(2)}, \delta f_i^{(3)})$ be the strain-energy density, and

$$V^* = \int_\Omega V d\Omega - \int_S (f_i^{(1)}u_i^{(1)} + f_i^{(2)}u_i^{(2)} + f_i^{(3)}u_i^{(3)})dS, \tag{B2}$$

be the complementary energy. Strictly, V should be the complementary strain-energy density; however, for linear stress–strain relations, V is equal to the strain-energy density.[17] The complementary energy theorem states that of all sets of forces that satisfy the equations of equilibrium and boundary conditions, the actual one that is consistent with the prescribed displacements is obtained by minimizing the complementary energy.[17] Then, $\delta V^* = 0$, and

$$\int_\Omega \delta V d\Omega = \int_S (\delta f_i^{(1)}u_i^{(1)} + \delta f_i^{(2)}u_i^{(2)} + \delta f_i^{(3)}u_i^{(3)})dS. \tag{B3}$$

We have from Eq. (B1)

$$\delta f_i^{(1)} = (1-I)\delta\tau_{ij}^{(1)}n_j,$$

$$\delta f_i^{(2)} = -\phi_w \delta p_f \delta_{ij}n_j,$$

$$\delta f_i^{(3)} = I\delta\tau_{ij}^{(3)}n_j. \tag{B4}$$

Substituting these expressions into (B3) yields

$$\int_\Omega \delta V d\Omega = \int_S [(1-I)(\delta\tau_{ij}^{(1)} - \phi_w \delta p_f \delta_{ij})u_i^{(1)} + I(\delta\tau_{ij}^{(3)} - \phi_w \delta p_f \delta_{ij})u_i^{(3)} - \delta p_f \delta_{ij}w_i]n_j dS, \tag{B5}$$

where w_i is given in Eq. (4). Applying Green's theorem to the surface integral, we obtain

$$\int_\Omega \delta V d\Omega = \int_\Omega [(1-I)(\delta\tau_{ij}^{(1)} - \phi_w \delta p_f \delta_{ij})u_i^{(1)} + I(\delta\tau_{ij}^{(3)} - \phi_w \delta p_f \delta_{ij})u_i^{(3)} - \delta p_f \delta_{ij}w_i]_{,j} d\Omega. \tag{B6}$$

Because the system is in equilibrium before and after the perturbation, and the fluid pressure is constant in Ω, the stress increments must satisfy

$$(\delta\tau_{ij}^{(1)})_{,j} = 0, \quad (\delta\tau_{ij}^{(3)})_{,j} = 0, \quad (\delta p_f \delta_{ij})_{,j} = 0, \tag{B7}$$

and we can write

$$\int_\Omega \delta V d\Omega = \int_\Omega [(1-I)(\delta\tau_{ij}^{(1)} - \phi_w \delta p_f \delta_{ij})\epsilon_{ij}^{(1)} + I(\delta\tau_{ij}^{(3)} - \delta p_f \delta_{ij})\epsilon_{ij}^{(3)} + \zeta \delta p_f]d\Omega. \tag{B8}$$

J. Appl. Phys., Vol. 94, No. 12, 15 December 2003

Carcione *et al.* 7847

The symmetry of the stress tensor has been used to obtain the relation $(u_i^{(m)} \delta \tau_{ij}^{(m)})_{,j} = \epsilon_{ij}^{(m)} \delta \tau_{ij}^{(m)}$. We finally deduce from (B8) that

$$\delta V = (1-I) \delta (\tau_{ij}^{(1)} - \phi_w p_f \delta_{ij}) \epsilon_{ij}^{(1)}$$
$$+ I \delta (\tau_{ij}^{(3)} - \phi_w p_f \delta_{ij}) \epsilon_{ij}^{(3)} + \delta p_f \zeta. \tag{B9}$$

APPENDIX C: FRACTAL POROSITY

We model fractal variations of porosity by using the von Kármán autocovariance function. Let ϕ_w be the average porosity (water proportion) and let $\Delta \phi$ be the maximum deviation of the porosity field from the background value ϕ_w. The porosity field at (x,y,z) is first subjected to the variations $(\Delta \phi_w)^r$, such that

$$-\Delta \phi \leq (\Delta \phi_w)^r \leq \Delta \phi, \tag{C1}$$

where $(\Delta \phi_w)^r$ is obtained from a random generator (the superscript "r" denotes random). Random numbers between 0 and 1 are generated and then scaled to the interval $[-1,1]\Delta \phi$.

Fractal variations of a given property are well described by the von Kármán autocovariance function.[18] The corresponding wave number–domain power spectrum is

$$P(k_x, k_y, k_z) = (1 + k^2 a^2)^{-(\nu + N/2)}, \tag{C2}$$

where $k = \sqrt{k_x^2 + k_y^2 + k_z^2}$ is the wave number, a is the correlation length, $\nu \, (0 < \nu < 1)$ is a self-similarity coefficient, and N is the Euclidean dimension. The von Kármán correlation function describes self-affine, fractal processes of fractal dimension $N + 1 - \nu$ at a scale smaller than a.

The porosity is then calculated as

$$\phi_w \pm \Delta \phi_w (x,y,z), \tag{C3}$$

where

$$\widetilde{\Delta \phi_w}(k_x, k_y, k_z) = (\widetilde{\Delta \phi_w})^r (k_x, k_y, k_z) P(k_x, k_y, k_z), \tag{C4}$$

with $(\widetilde{\Delta \phi})^r(k_x, k_y, k_z)$ being the Fourier transform of $(\Delta \phi_w)^r(x,y,z)$. (The tilde denotes the space Fourier transform.)

[1] J. L. Morack and J. C Rogers, Arctic **34**, 166 (1981).
[2] J. M. Carcione and U. Tinivella, Geophysics **65**, 54 (2000).
[3] S. Lee, P. Cornillon, and O. H. Campanella, 2002 Annual Meeting and Food Expo, Anaheim, CA.
[4] S. Jivanuwong, P. Mallikarjunan, and C. G. Haugh, 2002 Annual Meeting and Food Expo, Anaheim, CA.
[5] A. Timur, Geophysics **33**, 584 (1968).
[6] J. M. Carcione and G. Seriani, Geophys. Prospect. **46**, 441 (1998).
[7] P. Leclaire, F. Cohen-Ténoudji, and J. Aguirre-Puente, J. Acoust. Soc. Am. **96**, 3753 (1994).
[8] J. M. Carcione and G. Seriani, J. Comput. Phys. **170**, 676 (2001).
[9] M. A. Biot, J. Acoust. Soc. Am. **28**, 168 (1956).
[10] M. A. Biot, J. Appl. Phys. **33**, 1482 (1962).
[11] J. E. Santos, J. Douglas, Jr., J. Corberó, and O. M. Lovera, J. Acoust. Soc. Am. **87**, 1439 (1990).
[12] J. M. Carcione, *Wave Fields in Real Media: Wave Propagation in Anisotropic, Anelastic and Porous Media* (Pergamon, New York, 2001).
[13] F. Gassmann, Vierteljahrsschrift Naturforschenden, **96**, 1 (1951).
[14] J. E. Santos, C. L. Ravazzoli, and J. M. Carcione (unpublished).
[15] J. M. Carcione and H. B. Helle, J. Comput. Phys. **154**, 520 (1999).
[16] K. W. Winkler, J. Geophys. Res. **90**, 6793 (1985).
[17] Y. C. Fung, *Solid Mechanics* (Prentice-Hall, Englewood Cliffs, NJ, 1965).
[18] K. Holliger, Geophys. J. Int. **128**, 65 (1997).